Pergamon

Ocean Engineering 28 (2001) 957–987

OCEAN ENGINEERING

Wavelet analysis for processing of ocean surface wave records

Stanisław R. Massel *

Institute of Oceanology, Powstańców Warszawy 55, 81-712 Sopot, Poland

Received 3 March 2000; accepted 19 April 2000

Abstract

Wavelet analysis is a relatively new technique and in the recent years enormous interest in application of wavelets has been observed. This modern technique is particularly suitable for non-stationary processes as in contrast to the Fourier transform, (FT), the wavelet transform (WT) allows exceptional localization, both in time and frequency domains. The wavelet transform has been successfully implemented in signal and image processing, ordinary and partial differential equation theory, numerical analysis, communication theory and other fields. On the other hand, the application of the WT to ocean engineering and oceanography is rare. In this paper the WTs capability to give a full time–frequency representation of the wave signals is demonstrated. The processing of the time series of the non-stationary deep water waves, waves breaking at the tropical coral reefs and mechanically generated waves in the wave flume demonstrates the ability of the wavelet transform technique to detect a complex variability of these signals in the time–frequency domain. Various spectral representations resulting from the wavelet transform are discussed and their application for wave signals is shown.

Keywords: Wavelet transform; Fourier transform; Ocean surface waves; Spectral analysis; Wave measurement; Non-stationary signals

1. Introduction

Most oceanographic signals are the time-domain signals. However, in many cases the most distinguished information is hidden in the frequency spectrum which pro-

* Fax: +48-58-551-2130.
E-mail address: smas@iopan.gda.pl (S.R. Massel).

0029-8018/01/$ - see front matter
PII: S0029-8018(00)00044-5

vides the energy associated with a given frequency. The frequency spectrum of the signal can be obtained by the Fourier transform. The FT yields information on how much but not when (in time) the particular frequency components exist. Such information is sufficient in a case of the stationary signals as the frequency content of such signals does not change in time and all frequency components exist all the time.

However, in some cases the surface waves change in a relatively short period of time. Let us consider, for example, wave oscillations at a given point in the deep sea. The wave generation theory suggests that resulting wave frequencies depend on the wind speed, V, and its fetch, X, through the non-dimensional combinations, $\frac{gX}{V^2}$, and $\frac{gt}{V}$ (Massel, 1996). If a strong meteorological front is fast moving over the particular point of sea surface, the frequency content of the wave record at that point can change in a short period of time.

Another example are waves approaching the breaking stage. When waves start to break, the frequency content of signal changes rapidly in time due to nonlinear interaction between elementary wave components and resulting energy transfer, and energy dissipation. In such cases, the FT provides information on the frequency content, however, the information on the frequency localization in time is essentially lost in the process.

When the time localization of the spectral components is required, the transform of time series which provides the time–frequency representation of the signal should be developed. Transform of such type is the wavelet transform which gives full time–frequency representation of the time series. In contrast to the Fourier transform, the wavelet transform allows exceptional localization in the time domain via translations of the so called *mother wavelet*, and in the scale (frequency) domain via dilations (Combes et al., 1989; Farge, 1992; Kaiser, 1994; Torrence and Compo, 1998).

Wavelet transform is a relatively new technique and in recent years enormous interest in the application of wavelets has been observed. Wavelets have been successfully implemented in signal and image processing, ordinary and partial differential equation theory, numerical analysis and communication theory. On the other hand, the application of the wavelet transform to ocean engineering and oceanography is not frequent. Meyers et al. (1993) demonstrated the usefulness of the wavelet transform in studying dispersion of the Yanai waves in a reduced gravity equatorial model. In the paper by Shen and Mei (1994), the continuous wavelet transform was developed to analyze the energy balance in the equilibrium spectral subrange of the wind-generated gravity waves. Mori and Yasuda (1994) and Liu (1995) applied the wavelet transform to detect wave growth and breaking in the time series. A sudden surface jump associated with a breaking wave is regarded as a shock wave and the wavelet spectrum is defined to detect the occurrence of the surface jumps.

Atmospheric cold fronts observed in the boundary layer represent relatively sharp transition zones between air masses of different physical characteristics. Gamage and Blumen (1993) demonstrated the wavelet transform technique capability to detect

the cold-fronted features. Torrence and Compo (1998) in their practical step-by-step guide used the wavelet transform to give a quantitative measure of changes in the El Niño–Southern Oscillation (ENSO).

An intermittent feature of sea turbulence is a particularly suitable problem for application of the wavelet transform to detect the intermittency of energy input from wind to ocean surface (see, for example, papers by Farge, 1992; Shen and Mei, 1993). An application of the wavelet transform for identification of the energy cascade in the atmospheric turbulence was discussed by Yamada and Ohkitani (1990, 1991).

Unfortunately, not all above applications provide quantitative results. Due to lack of quantitative results, the wavelet transform has been regarded by many as an interesting tool to produce colourful pictures, yet purely qualitative results.

In this paper the application of wavelet transform for the processing of surface waves is discussed and an attempt to produce some useful quantitative results is made. The paper is organized as follows. In Section 2, a short overview of the Fourier transform is given. In Section 3, the theory of windowed Fourier transform and its resolution are discussed. In Section 4, the fundamentals of the wavelet transform are given and the difference between Fourier and wavelet transforms is demonstrated. The application of the wavelet transform for processing of the simple and real wave signals is shown in Sections 5 and 6, respectively. In particular, surface waves changing due to propagation of the fast atmospheric fronts, non-stationary evolution of waves close to the breaking point and in breaking zone, as well as evolution of mechanically generated waves in the wave flume are discussed. Finally, main conclusions of the paper are given in Section 7.

2. Overview of the Fourier transform

The Fourier transform is probably the most popular transform being used, but for better understanding the difference between the wavelet transform and the Fourier transform, let us provide a short overview of the Fourier transform. We start with a case of continuous deterministic signal $x(t)$. If the total signal energy, E, is finite or if:

$$E=\int_{-\infty}^{\infty}|x(t)|^2dt<\infty, \tag{1}$$

then $x(t)$ is absolute-integrable over the entire domain and the Fourier transform $X(f)$ of the $x(t)$ exists as follows:

$$X(f)=F[x(t)]=\int_{-\infty}^{\infty}x(t)\exp(-i2\pi ft)dt, \tag{2}$$

and

$$x(t)=F^{-1}[X(f)]=\int_{-\infty}^{\infty} X(f)\exp(i2\pi ft)df. \tag{3}$$

Using the square of the modules of the Fourier transform we obtain the energy spectral density of the signal in the form:

$$S(f)=X(f)X^*(f)=|X(f)|^2, \tag{4}$$

where the asterisk denotes the complex conjugate. The integration of the spectral density $S(f)$ over the entire spectral domain provides the total energy, E, of the signal:

$$\int_{-\infty}^{\infty}|X(f)|^2df=E=\int_{-\infty}^{\infty}|x(t)|^2dt. \tag{5}$$

This relationship is known as Parseval's theorem.

Let us suppose that $x(t)$ is a stationary random process. Unlike for the finite energy deterministic signal, the total energy in the stochastic process is unbounded and the transform of Eq. (2) does not exist, as the total energy given by Eq. (1) does not decrease because the length of the time series increases without bound. To overcome this problem, we must deal with the frequency distribution of the signal power, E/T, where T is the record time. Now the quantity, E/T, is a function bounded in time.

There are two different methods of the spectral analysis of stationary random processes, the first one based on the transformation of the autocorrelation function — Blackman–Tuckey method and the second one in which the transformation of the primary signal, $x(t)$, is used — Fast Fourier Transform (FFT) method (Bendat and Piersol, 1986; Massel 1996, 1999). The details of both methods are not discussed here.

In Fig. 1a, an example of a stationary signal, $x(t)$, being of a superposition of three sinusoidal components, is shown for the time domain $0<t<60$ s, i.e.:

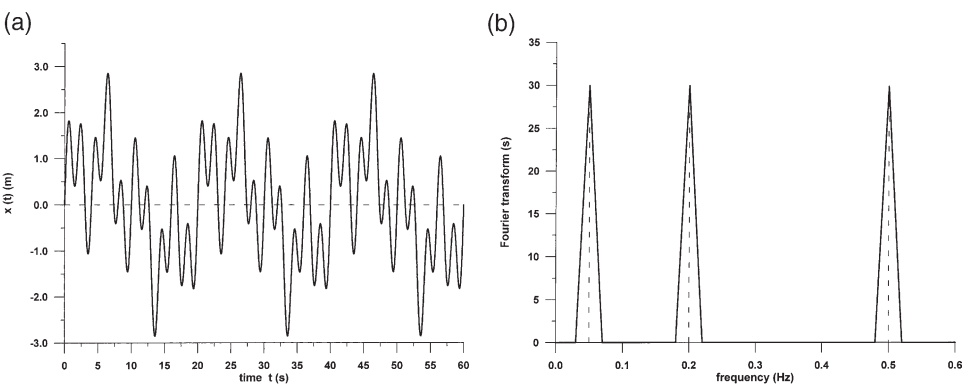

Fig. 1. The three-components sinusoidal signal: (a) time series, (b) Fourier Transform.

$$x(t) = \sin\left(\frac{2\pi t}{T_1}\right) + \sin\left(\frac{2\pi t}{T_2}\right) + \sin\left(\frac{2\pi t}{T_3}\right) = \sin(2\pi\cdot 0.5t) + \sin(2\pi\cdot 0.2t) + \sin(2\pi\cdot 0.05t), \tag{6}$$

in which T_1=2 s, T_2=5 s, and T_3=20 s.

The corresponding Fourier transform of the signal is given in Fig. 1b. The frequency content of the signal, $x(t)$, does not change in time, as should be expected. Therefore, one does not need to know when frequency components exist; they simply exist all the time. In other words, the Fourier transform gives us full information on the signal Eq. (6).

Now let us assume that the frequency content of the signal changes in time. An example of such a signal is shown in Fig. 2a. This is, so called, a *chirp* signal with three different frequency components existing at three different time intervals. In the interval 0 to 20 s, the 0.5 Hz sinusoid exists, the time interval 20 s to 40 s contains a 0.2 Hz sinusoid, while in the interval from 40 s to 60 s the frequency of sinusoid is 0.05 Hz. The corresponding Fourier transform is given in Fig. 2b. Similarly to Fig. 1b, the Fourier transform has three peaks at the frequencies 0.05, 0.2 and 0.5 Hz with reasonable amplitudes. The ripples in the figure are due to sudden changes from one frequency component to another. If these ripples are neglected, Figs. 1b and 2b become very similar. Therefore, the signals in Figs. 1a and 2a yield the same frequency structure when the Fourier transform approach is used. However, the signal given in Fig. 1a has these frequencies all the time, but the signal shown in Fig. 2a has them at different intervals of time. Thus, the Fourier transform gives a spectral content of the signal but no information when those spectral components appear. The Fourier transform can only be used if one is interested in what spectral components exist in the signal. If one wants to know what spectral component occurs at what time, or in case when the time localization of the spectral components is required, the Fourier transform is not a good choice.

In other words, in the Fourier transform there is no resolution problem in the

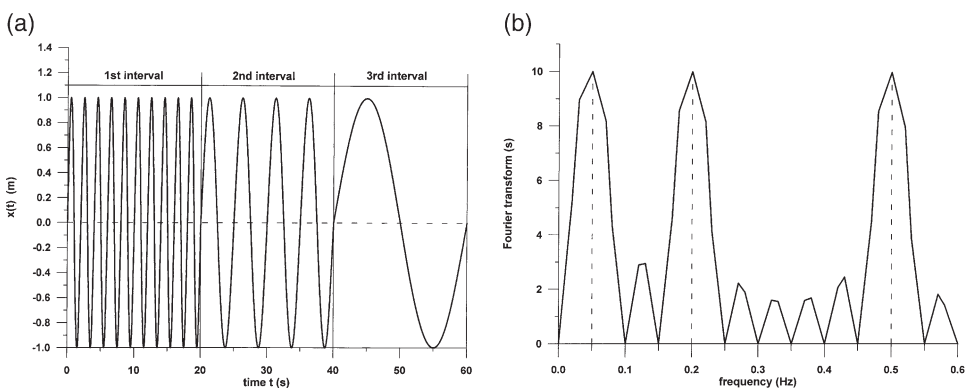

Fig. 2. "Chirp" type signal of three frequency components existing at different time: (a) time series, (b) Fourier transform.

frequency domain as we know exactly what frequencies exist. This perfect frequency resolution in the Fourier transform is due to the fact that the window, $\exp(i\omega t)$, used in this transformation, lasts all the time, from minus infinity to plus infinity. Similarly, there is no time resolution problem in the time domain, since we know the value of the signal at every instant of time. In contrary, we can say that both time resolution in the FT, and the frequency resolution in the time domain are zero, since we have no information about them.

3. Windowed Fourier transform (WFT)

The most obvious choice to insert time information into the frequency domain of the signal, $x(t)$, is to divide the signal into segments small enough so that the signal can be assumed to be stationary. For each such segment, the Fourier transform can be applied. For this purpose, so called window function, w, is chosen. A commonly used window function is a boxcar window without smoothing or a Gaussian function of the form:

$$w(t)= \exp\left[-\frac{t^2}{2a}\right], \tag{7}$$

in which a determines the width of the window. It is clear that the width of the window should be equal to the segment of the signal where stationarity is assumed. The window function and the signal are multiplied and the product is treated as another signal for which the Fourier transform is taken. This approach is known as the Windowed Fourier Transform (WFT). Let us assume that the width of the window is T. Thus, for a given time instant, t_0, the window function overlaps the time interval $(t_0-T/2,\ t_0+T/2)$. Within this interval, the multiplication of the signal, $x(t)$, and the window, w, and the integration of the product provides the WFT for time t_0. In the next step, the window is shifted by time step Δt to a new location until the end of the signal. The total procedure to determine the WFT can be summarized as follow:

$$WFT(\tau,f)=\int_t [x(t)w^*(t-\tau)]\exp(-i2\pi ft)dt, \tag{8}$$

in which the asterisk denotes the complex conjugate quantity. For every time, τ, and frequency, f, a new WFT coefficient is computed and two dimensional time-frequency transformation of the signal is obtained.

In contrast to the Fourier transform, in the windowed Fourier transform the window is of finite length, so we have no perfect frequency resolution. When we assume that the length of the window is infinite, just like for the Fourier transform, we obtain a perfect frequency resolution, but the time information will be totally lost. To obtain a stationary record, the window in which the signal is stationary, should be short enough. The narrower we make the window, the better the time resolution, but the frequency resolution becomes poorer.

The selection of the proper window width is related to what is known as the Heisenberg Uncertainty Principle (Van Name, 1960). This principle, originally applied to the momentum and location of moving particles in quantum mechanics, can also be applied to time–frequency information of a signal. We do not know what spectral components exist at what instances of time. Narrow windows give a good time resolution, but poor frequency resolution. Wide windows give good frequency resolution, but poor time resolution. Furthermore, wide windows may violate the condition of stationarity. The wavelet transform, described in the next Section, solves the dilemma of resolution in the time–frequency domain to a certain extent.

4. Wavelet transform

4.1. Basic definitions and properties

The wavelet analysis is similar to the Fourier analysis as it breaks a signal down into its constituents. Whereas the Fourier transform breaks the signal into a series of sine waves of different frequencies, the wavelet transform breaks the signal into its *wavelets* which are scaled and shifted versions of the so called *mother wavelet*. The wavelet transform allows exceptional localization both in the time domain via translations of the wavelet, and in the frequency (scale) domain via dilations.

The wavelet transforms are proposed in papers of Morlet, Meyer, Grossman, Mallat and others (Meyer et al., 1987; Combes et al., 1989; Tuteur, 1989; Farge, 1992; Daubechies, 1992). The wavelets are complex or real functions concentrated in time and frequency and having the same shape. In the wavelet analysis, the signal is multiplied with the wavelet, and the transform is separately computed for different segments of the time domain signal. In general, the wavelet transform (WT) of the signal, $x(t)$, is defined as a following inner product:

$$WT(\tau,b)=<g_{\tau b}|x>=\int_{-\infty}^{\infty} x(t)g^{*}_{\tau b}(t;\tau,b)dt. \tag{9}$$

The family of continuously translated and dilated wavelets is generated from mother wavelet $g(t)$:

$$g_{\tau b}(t;\tau,b)=\frac{1}{\sqrt{b}}g\left(\frac{t-\tau}{b}\right), \tag{10}$$

where τ is the translation parameter, corresponding to the position of the wavelet as it is shifted through the signal, b is the scale dilation parameter determining the width of the wavelet. The scale $b>1$ dilates (or stretches out) the signals, whereas scale $b<1$ compresses the signal. The wavelet coefficients, $WT(\tau,b)$, represent the correlation (in terms of the time-scale functions) between the wavelet and a localized

section of the signal. If the signal has a major component of the frequency corresponding to the given scale, then the wavelet at this scale is close to the signal at the particular location and the corresponding wavelet transform coefficient, determined at this point, has a relatively large value. Therefore, the wavelet transform is a sort of *microscope* with magnification $1/b$ and location given by parameter τ, while the optics of the microscope is characterized by the function $g_{\tau b}(t;\tau,b)$.

For the wavelet which has the mother wavelet status, the function $g(t)$ must satisfy several properties, such as (Farge, 1992; Emery and Thomson, 1997):

1. The amplitude $|g(t)|$ must decay rapidly to zero in the limit $|t|\rightarrow\infty$. This feature ensures the localization aspect of wavelet analysis. It means that the wavelet $g[(t-\tau)/b]$ has insignificant effect at time $|t|>\tau_{\text{crit}}$, where τ_{crit} is a critical time lag.
2. The wavelet $g(t)$ must have zero mean. This condition, known as the admissibility condition, ensures the invertibility of the wavelet transform. Thus, the original signal can be obtained from the wavelet coefficients through the inverse transform (Emery and Thomson, 1997):

$$x(t)=\frac{1}{C}\int_{-\infty}^{\infty}\int_{-\infty}^{\infty} WT(\tau,b)b^{-2}g_{\tau b}\,d\tau\,db, \tag{11}$$

in which:

$$C^{-1}=\int_{-\infty}^{\infty}(\omega^{-1}|G(\omega)|^2)\,d\omega, \tag{12}$$

and the $G(\omega)$ is the Fourier transform of function $g(t)$.

3. The wavelets are regular functions such that $G(\omega<0)=0$. It means that wavelets need to be described in terms of positive frequencies only.

Determination of the wavelet transform by the integral Eq. (9) is the simplest but the most time-consuming method. When we integrate in the translation-scale domain (τ,b), where $0<b<M\Delta t_b$ and $0<\tau<N\Delta t_\tau$, the integration time of MN^2 is needed. The Δt_b is the scale step and Δt_τ is the time lag step. Another method is based on the convolution theorem and spectral representation of the wavelet transform (Farge, 1992; Emery and Thomson, 1997), i.e.:

$$WT(\tau,b)=\sqrt{b}\int_{-\infty}^{\infty}\exp(i\tau\omega)G^*(b\omega)X(\omega)\,d\omega, \tag{13}$$

in which $G(\omega)$ and $X(\omega)$ are the Fourier transforms of $g(t)$ and $x(t)$, respectively. Using the FFT procedure the integration time is reduced to $MN \log_2 N$.

The wavelet transform should reflect the type of features which are present in the time series. For time series with sharp steps, a boxcar-like wavelet should be chosen, while for smoothly varying time series a smooth function is more appropriate. However, if the wavelet power spectra are not of the primary interest, the choice of wavelet function is not critical.

One of the most extensively used mother wavelet is the Morlet's wavelet:

$$g(t) = \exp\left(-\frac{1}{2}t^2\right)\exp(ict). \tag{14}$$

Eq. (14) represents a plane wave of frequency c, modulated by a Gaussian envelope of the unit width. For calculations in this paper only wavelet Eq. (14) is used. In the oceanographic applications, the other mother wavelets, such as the orthogonal wavelets (Yamada and Ohkitani 1990, 1991; Mori and Yasuda, 1994), Paul's wavelet or DOG wavelet (derivative of a Gaussian) (Torrence and Compo, 1998) are also used.

Using the representation Eq. (10), the Morlet wavelet takes the form:

$$g_{\tau b}(t) = \frac{1}{\sqrt{b}}\exp\left[-\frac{1}{2}\left(\frac{t-\tau}{b}\right)^2\right]\exp\left[ic\frac{t-\tau}{b}\right]. \tag{15}$$

The frequency nature of the parameter c is clearly seen if we take $c=2\pi$. Then Eq. (15) becomes:

$$g_{\tau b}(t) = \frac{1}{\sqrt{b}}\exp\left[-\frac{1}{2}\left(\frac{t-\tau}{b}\right)^2\right]\exp\left[i\frac{2\pi}{b}(t-\tau)\right]. \tag{16}$$

Now the term $\exp\left[i\frac{2\pi}{b}(t-\tau)\right]$ represents the plane sinusoidal wave of a frequency $2\pi/b$; thus the scale dilation b can be treated as a period.

The real and imaginary parts of the wavelet Eq. (16) for various scale parameters b are illustrated in Figs. 3a, b and 4a. As b increases, the width of the Gaussian spreads in time from its centre value. If the scale parameter, b, is constant and frequency parameter, c, increases, the number of oscillations over the span of the function also increases. This effect is clearly seen when comparing Figs. 4a, b and c.

Once a wavelet function is chosen, it is necessary to use a set of scales, b, in the wavelet transform Eq. (16) to build up a more complete picture. It is convenient to adopt the scale b as functional powers of two (Torrence and Compo, 1998):

$$b_i = b_0 2^{i\delta}, \quad i=0,1,\ldots,M, \tag{17}$$

in which

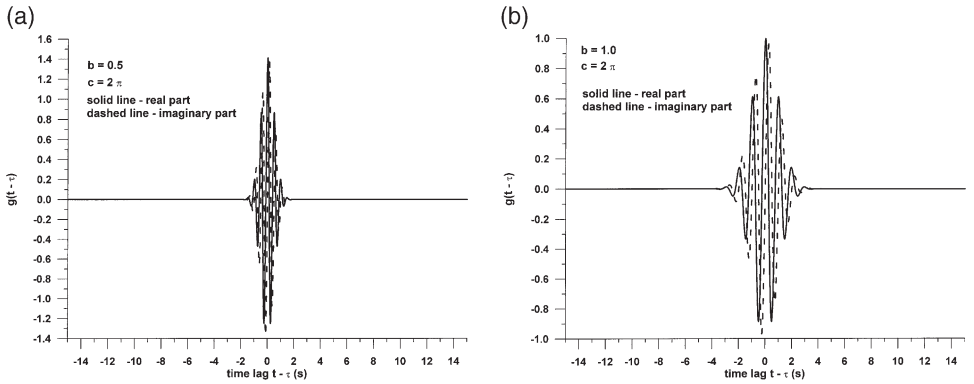

Fig. 3. The Morlet's wavelet Eq. (15) of a constant c and different scales b: (a) b=0.5, c=2π; (b) b=1.0, c=2π.

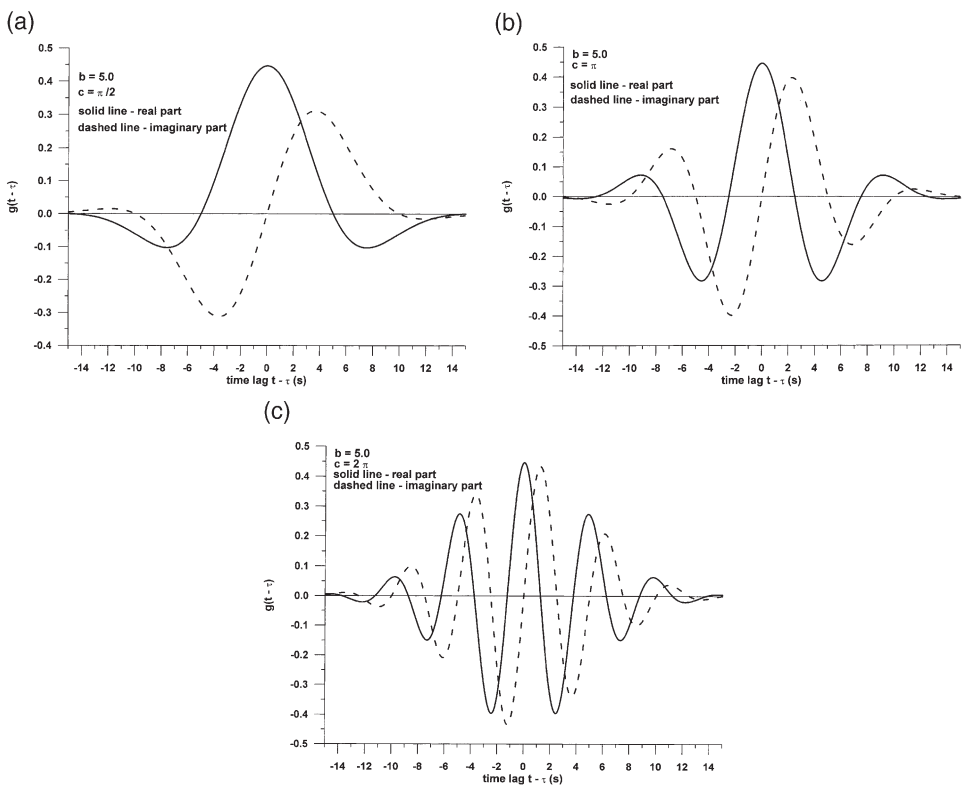

Fig. 4. The Morlet's wavelet Eq. (15) of a constant scale b and different c parameters: (a) b=5.0, c=π/2; (b) b=5.0, c=π; (c) b=5.0, c=2π.

$$M=\frac{1}{\delta}\log_2\left(\frac{N\Delta t}{b_0}\right), \tag{18}$$

where N is the number of values in the time series, and Δt is the time sampling. The b_0 is the smallest reasonable scale while b_M determines the largest scale. The b_0 should be chosen of such a value to let the equivalent Fourier period (see Section 4.2) to be equal to approximately $2\Delta t$. The scale factor δ should be chosen to provide adequate sampling in scale b. For the Morlet wavelet, δ of about 0.5 is the largest value that still gives a smooth picture of the wavelet spectrum. However, smaller values of δ give finer resolution. In this paper, except the scales b chosen according to Eq. (17), the linear set of scales will be used, i.e.:

$$b_i=b_0+\Delta bi. \tag{19}$$

The wavelet analysis is done in a similar way to the WFT analysis in the sense that the signal is multiplied with a window (the wavelet). However, the window width has been changed as the transform is computed for every single spectral component. This is the most significant characteristic of the wavelet transform. Changing the window width influences the resolution of the transform, which is illustrated in Fig. 5. Every box corresponds to the value of the wavelet transform in the translation-scale plane. Although the widths and heights of the boxes change, their areas are constant (see two hatched boxes in Fig. 5). Each box represents the same portion of the time-frequency plane, but gives different ratios of time and frequency. At low frequency (high value of scale b), the height of the box is small, but its width is large, i.e. the frequency resolution is better but time resolution is poor (more ambiguity regarding the value of the exact time). On the other hand, at higher frequencies (low scale s), the height of the boxes increases and the width of the boxes decreases. This corresponds to a very narrow window when the frequency resolution is poorer and the time resolution is better.

In the WFT, the time and frequency resolutions are determined by constant width of the window, i.e. both time and frequency resolutions are constant. Therefore in the WFT case the time–frequency plane consists of rectangles. However, as we mentioned in Section 3, the areas of the boxes due to the Heisenberg's Uncertainty Principle can not be reduced as much as we want. In case of wavelets, the dimensions of the boxes can be changed, with the same area. This is the main advantage of the wavelet transform over the windowed Fourier transform.

Now let us examine some energy properties of the wavelet transform. First, the wavelet transform conserves the total energy, i.e.:

$$\int_{-\infty}^{\infty}|x(t)|^2dt=C^{-1}\int_0^{\infty}\int_0^{\infty}|WT(\tau,b)|^2b^{-2}d\tau db, \tag{20}$$

in which the coefficient C is given by Eq. (12).

Using the wavelet transform and the coefficient C we can define the various wave-

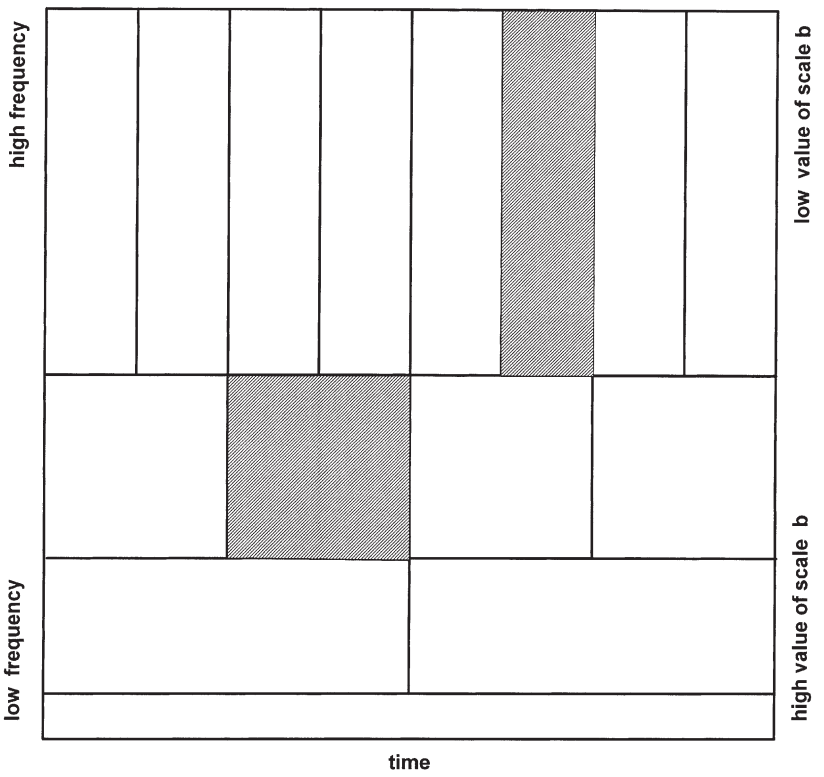

Fig. 5. Resolution scheme in the time–frequency plane.

let energy spectra and spectral densities. In particular, the so called, *time-scale energy density* becomes:

$$E_1(\tau,b)=\frac{|WT(\tau,b)|^2}{b}. \tag{21}$$

By integrating Eq. (21) versus scale b, we obtain the *local energy density* (Farge, 1992):

$$E_2(\tau)=C^{-1}\int_0^{\infty} E_1(\tau,b)\frac{db}{b}. \tag{22}$$

On the other hand, the integration of Eq. (21) versus time τ, gives the *global wavelet energy spectrum* $E_3(b)$ as:

$$E_3(b)=\int_0^{\infty} E_1(\tau,b)d\tau. \tag{23}$$

Torrence and Compo (1998) noted that the smoothed Fourier spectrum approaches the global wavelet spectrum when the amount of necessary smoothing decreases with increasing scale. Moreover, Percival (1995) showed that the global wavelet spectrum provides an unbiased and consistent estimation of the true power spectrum.

Finally, the *total energy* of the time series $x(t)$ becomes:

$$E=C^{-1}\int_0^{\infty} E_3(b)\frac{db}{b}. \tag{24}$$

After substituting Eqs. (21) and (23) into Eq. (24) we get:

$$E=C^{-1}\int_0^{\infty}\int_{-\infty}^{\infty} E_1(\tau,b)\frac{d\tau db}{b}=C^{-1}\int_0^{\infty}\int_{-\infty}^{\infty}|WT(\tau,b)|^2\frac{d\tau db}{b^2}, \tag{25}$$

which confirms the conservation of energy Eq. (20).

4.2. Resemblance of wavelets to Fourier modes

For a better understanding of the wavelet transform nature, the relation between the wavelet transform and the more common Fourier transform is the basic one for the interpretation of the results of processing of the signals by the wavelet technique. This relation is not straightforward for arbitrary wavelet. However, in the case of the Morlet wavelet used in this paper, the relationship between WT and FT can be found in a simpler way, mainly due to the periodic character of the Morlet's wavelet (Meyers et al., 1993). Let us assume the periodic wave train of the frequency ω_0 and unit amplitude, i.e.:

$$x(t)=\exp(\omega_0 t). \tag{26}$$

The Fourier transform of signal Eq. (26) is $X(\omega)=F[x(t)]=\delta(\omega-\omega_0)$, where $\delta()$ is the Dirac's delta function. Using Eq. (13) we have:

$$WT(\tau,b)=\sqrt{b}\int_{-\infty}^{\infty}\exp(i\tau\omega)G^*(b\omega)\delta(\omega-\omega_0)d\omega=\sqrt{b}\exp(i\tau\omega_0)G^*(b\omega_0). \tag{27}$$

Thus,

$$|WT(\tau,b)|^2 = b|G^*(b\omega_0)|^2. \tag{28}$$

On the other hand, the Fourier transform $|G^*(b\omega_0)|$ of the Morlet's wavelet Eq. (14) is:

$$|G^*(b\omega_0)| = \exp[-(b\omega_0 - c)]. \tag{29}$$

Substituting Eq. (29) into Eq. (28) we obtain:

$$|WT(\tau,b)|^2 = b \exp[-(b\omega_0 - c)^2]. \tag{30}$$

A condition which yields the maximum correlation between the wavelet and a Fourier component of frequency, ω_0, is given by:

$$\frac{\partial[|WT(\tau,b)|^2]}{\partial b} = 0, \tag{31}$$

or

$$-2\omega_0^2 b^2 + 2c\omega_0 b + 1 = 0. \tag{32}$$

The only realistic solution of Eq. (32) is:

$$b = \frac{1}{2}\left[\frac{c}{\omega_0} + \frac{\sqrt{c^2+2}}{\omega_0}\right]. \tag{33}$$

As $\omega_0 = \frac{2\pi}{T_0}$, Eq. (33) yields a linear relationship between scale, b, and period, T_0, in the form:

$$b = \frac{c+\sqrt{c^2+2}}{4\pi} T_0 = \alpha T_0, \tag{34}$$

where

$$\alpha = \frac{c+\sqrt{c^2+2}}{4\pi}. \tag{35}$$

Again, Eq. (34) indicates that physical dimension of scale, b, is the time. Assuming that $c=2\pi$, Eq. (35) yields $\alpha=1.0125$. The scale, b, becomes fully equivalent to the

period T_0 (α=1) when $c=\frac{[(4\pi)^2-2]}{8\pi}\approx 6.2036$. Using a fact that the difference between $c=2\pi$ and c=6.2036 is very small, in the application discussed in Sections 5 and 6, the value $c=2\pi$ is used. Such choice of c value underlines the oscillatory nature of the second term of the Morlet wavelet Eq. (16) which is very suitable for processing of the ocean wave data. Thus, for the Morlet wavelet, the scale b and the Fourier period T are nearly identical. In plottings in this paper, for better interpretation of the wavelet analysis both wavelet scale, b, and the equivalent Fourier period, T, are shown. However, it should be noted that for other mother wavelets, the Fourier period differs from scale, b. For example, for the Mexican hat, the Fourier period, T, is four times larger than the scale, b.

From the definition of WT, given by Eq. (9), it follows that any linear superposition of periodic modes results in separate local maxima, as described above. Thus, for any function of the type:

$$x(t)=\sum_n A_n \exp(i\omega_n t), \tag{36}$$

the WT has modulus maxima at:

$$b_n=\frac{c+\sqrt{c^2+2}}{4\pi}T_n. \tag{37}$$

Although wavelets have a definite scale and some correspondence between scales and Fourier periods exist, there is no resemblance to Fourier modes.

5. Application of wavelet transform for processing of simple signals

Before applying the WT technique to more complex signals resulting from oceanographic data, the simpler signals are discussed. Let as assume the sinusoidal signal $x(t)$ as:

$$x(t)=1.0\cdot \sin\left(\frac{2\pi t}{T}\right) \text{ for } 10\text{s}<t<16\text{s}, \tag{38}$$

where T=2 s. In Fig. 6a, the absolute value of wavelet transform $|WT|$ for three different scales b=1.0 s, 2.0 s and 2.5 s, corresponding to the Fourier periods 0.987 s, 1.975 s and 2.439 s, is shown. The maximum values of the WT appears at the wave crests and wave troughs (i.e. at time instants with max denivelations of the wave profile) when the scale parameter, b, is approximately equal to the period of the input signal T=2 s. On the other hand, the wavelet transform becomes zero at the points where surface elevation is zero, i.e. at t=11, 12, 13 s etc.

In general, when dealing with the finite-length time series, some errors occur at

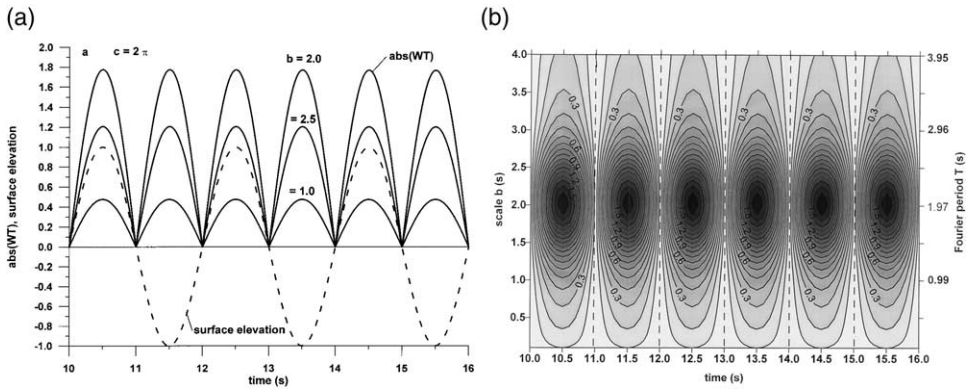

Fig. 6. Absolute values of the wavelet transform of simple sinusoidal signal: (a) $|WT|$ as a function of time for particular values of scale b (b) contours of the $|WT|$.

the beginning and the end of the wavelet spectrum. These regions of the spectrum in which edge effects become important are known as the *cone of influence*. Torrence and Compo (1998) define it as, so called, e-folding time which ensures that the wavelet spectrum at the edge drop by a factor $\exp^{-2}$ and the edge effect beyond this point are negligible. However, for cyclic series, as in Eq. (38), there is no cone of influence.

The contours of the function $|WT(\tau,b)|$ for the sinusoidal signal Eq. (38) and for scales 0.1 s$<b<$4.0 s are shown in Fig. 6b. The right axis is the Fourier period, T, (in seconds) corresponding to the wavelet scale, b, (in seconds) shown on the left axis. The dashed lines indicate the time instants at which $|WT|$ becomes zero.

In Fig. 7 another example of the wavelet transform for time series $x(t)$ being a superposition of three sinusoidal signals is given:

$$x(t)=\sin\left(\frac{2\pi t}{2}\right)+\sin\left(\frac{2\pi t}{5}\right)+\sin\left(\frac{2\pi t}{10}\right). \tag{39}$$

As should be expected, the maxima of $|WT|$ correspond to the scale parameters b almost equal to the Fourier periods of the wave components, i.e. for b=2 s, 5 s and 10 s. The wavelet transform vanishes at t=5+5·n, where n=1,2,3,… (see dashed lines in Fig. 7).

Now, let us consider the "chirp" type signal. The frequency components, contributed to the signal, are the same as above, but appearing at three different time intervals, i.e.:

$$\zeta(t)=\begin{cases}1.0\cdot\sin\left(\dfrac{2\pi t}{2}\right) & \text{for } 5\text{s}<t<20\text{s},\\ 1.0\cdot\sin\left(\dfrac{2\pi t}{5}\right) & \text{for } 20\text{s}<t<40\text{s},\\ 1.0\cdot\sin\left(\dfrac{2\pi t}{10}\right) & \text{for } 40\text{s}<t<50\text{s}.\end{cases} \tag{40}$$

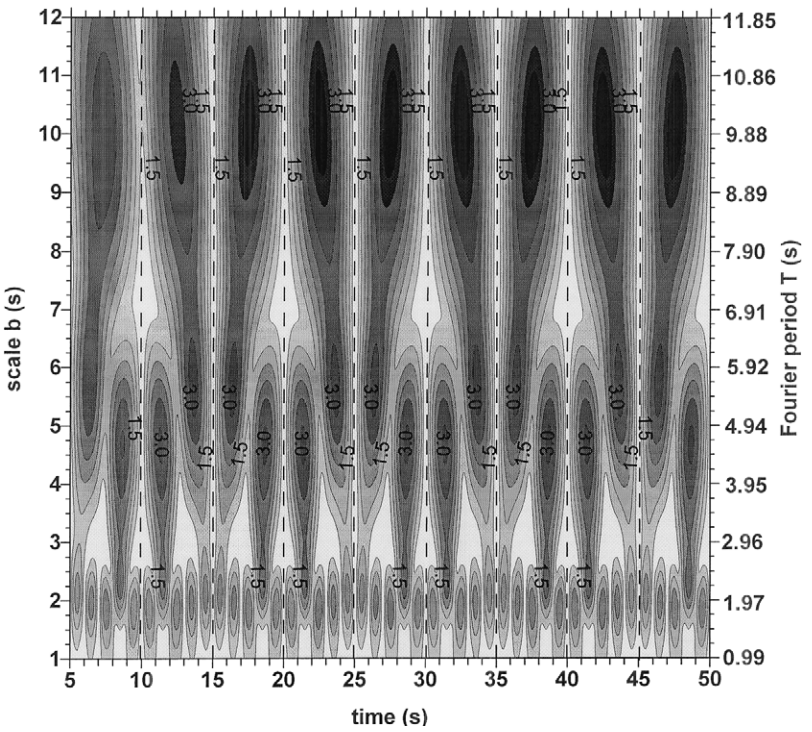

Fig. 7. Contours of the $|WT|$ for a superposition of three sinusoidal signals Eq. (39).

The absolute values of the wavelet transform are shown in Fig. 8. Maximum values of the $|WT|$ correspond to the scale parameters equivalent to the periods of signal components, as should be expected. However, the maximum values of $|WT|$ shift to the higher scales as the periods of the initial signal components increase. Fig. 8 demonstrates the wavelet transform capability to provide the time and frequency information simultaneously, giving a full time–frequency representation of the signal. In contrast to the Fourier transform, the wavelet transform allows exceptional localization both, in the time and in the (frequency) scale domains.

In order to calculate various types of wavelet densities and spectra, defined in Section 4.1, we apply the WT shown in Fig. 8. In Fig. 9, the *global wavelet energy spectrum* $E_3(b)$ is plotted versus the quantity $f=1/b$, which can be considered as a measure of frequency. The dominant contribution into the global wavelet spectrum is provided by the signal components with frequencies f=0.1 Hz, 0.2 Hz and 0.5 Hz, as should be expected. Although the spectrum E_3 mimics the common Fourier spectrum, there is not a straightforward correspondence between E_3 and frequency spectrum based on the Fourier transform.

The *local energy density* $E_2(\tau)$, corresponding to the time series Eq. (40), is shown in Fig. 10. The local spectrum $E_2(\tau)$ reflects the oscillating character of the initial

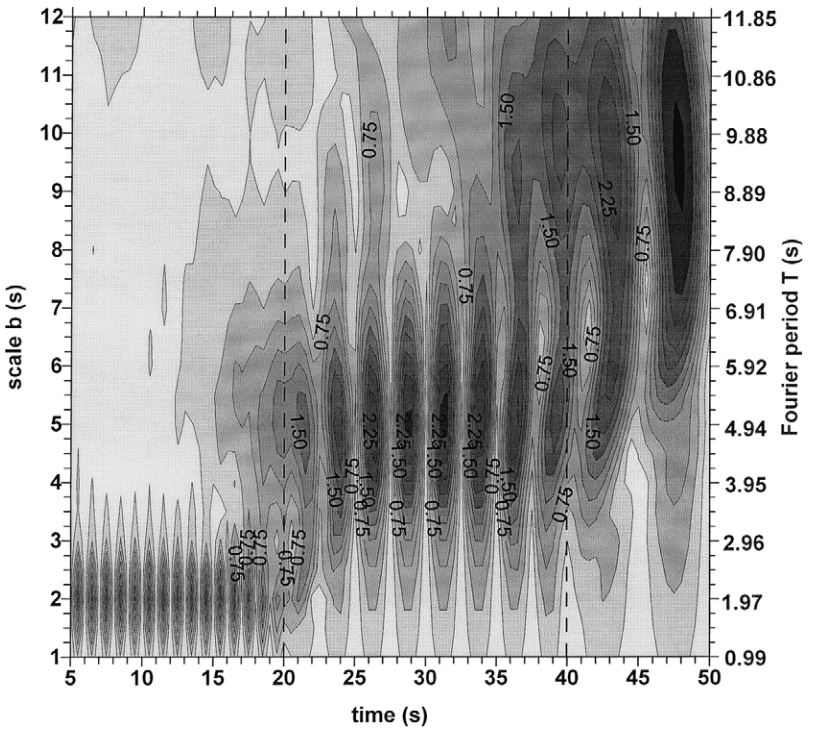

Fig. 8. Contours of the $|WT|$ for the "chirp" type signal Eq. (40).

time series. At the boundaries between these intervals, close to time τ=20 s and τ=40 s, the oscillations of the quantity $E_2(\tau)$ are substantially reduced. It should be noted that for the periodic time series with one frequency only, the local energy density, $E_2(\tau)$, vanishes at the time instants, τ, at which time series, $x(t)$, becomes zero.

6. Application of WT to real wave time series

In this section, the application of the wavelet transform to processing of the real wave data is demonstrated. First, a rapid evolution of the deep-water wave field, due to fast movement of the atmospheric front over the Baltic Sea, is discussed. The second example deals with the wave frequency structure transformation due to breaking on the top of the Ningaloo Reef in the Western Australia. Finally, a disintegration of the mechanically generated wave trains in the wave tank, in terms of the WT, is described.

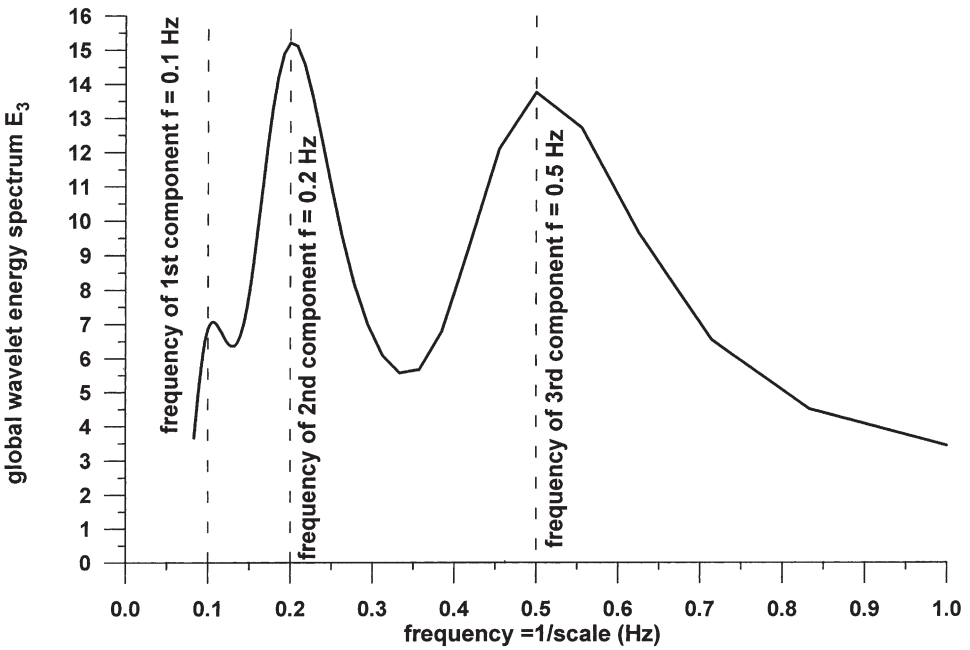

Fig. 9. Global wavelet energy spectrum E_3 for signal Eq. (40).

6.1. Wave growth due to fast moving atmospheric front

6.1.1. Remarks on experimental data

Wind blowing over the water surface generates waves. The stronger the wind is, the more energetic are the waves, and the wave generation process continues as long as the forcing is maintained. During wave experiments in nature, records of the sea surface are usually of the order of 20 min, and such records are treated as stationary. Time intervals between the particular records depends on dynamics of the growing waves and on the instruments used. This time interval is of the order of one to three hours. As a result, we obtain a set of stationary records of surface waves, each of the duration of about 20 min. These stationary records are subsequently processed using the classical Fourier transform techniques.

Due to the intermittent nature of wave recording, we are not able to make any conclusion, whether the wave field is stationary or not and how it evolves between the particular records. This can be done only through a continuous recording of the wave surface, changing quickly in time. In Fig. 11, a variation of the significant wave height, H_s, during one month (August 1998) is shown. Data are based on the wave record using the Datawell Waverider Buoy in the Baltic Sea (54° 51.234′ N, 17° 48.352′ E) at the depth of 20 m (Paplinska, 1999). In this paper, the attention is focused on one day only, i.e. August 9, 1998 (see Fig. 12). Closed circles indicate the calculated values, resulting from the time series of duration of 20 min, while the full lines are the interpolated values.

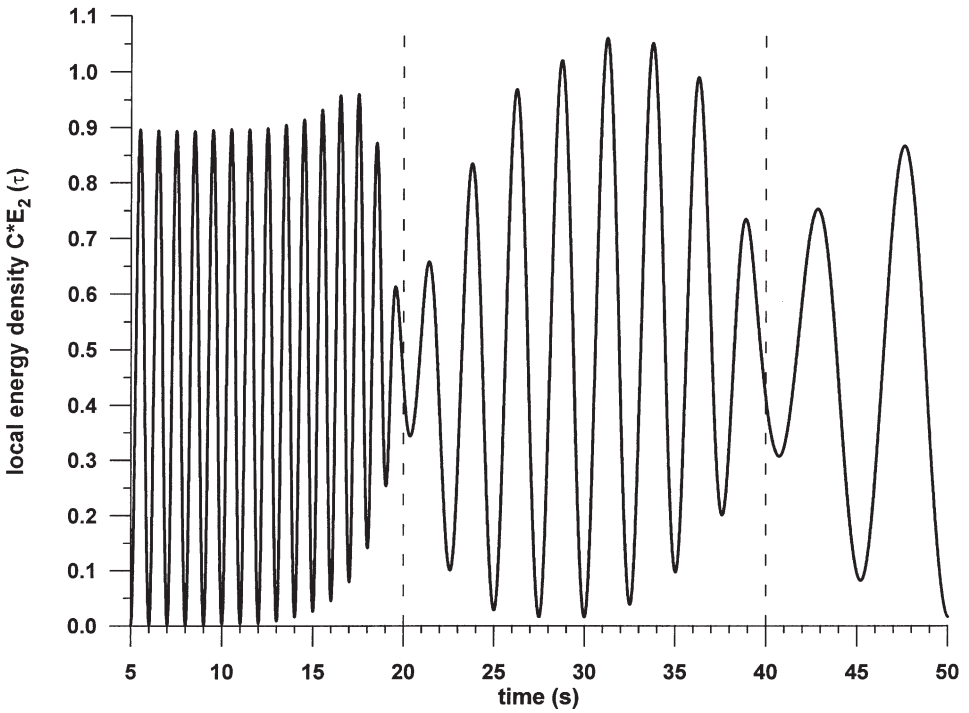

Fig. 10. Local energy density $C{\cdot}E_2(\tau)$ for signal Eq. (40).

6.1.2. Reconstructing of missing data

Let us form a continuous wave record for the first seven hours of August 9, 1998. During this time interval we had only five measurements, of 20 minutes each. Thus, we have to reconstruct the missing time series using the interpolated significant wave heights, H_s, and peak frequency, ω_p, values. For consistency, we assume that the duration of each of the reconstructed records is equal to 20 minutes, and the significant wave height and peak frequency are known. Moreover, let the spectral representation of the wave field be given by the JONSWAP spectrum with Kitaigorodskii's scaling due to finite water depth (Massel, 1996):

$$S(\omega)=\alpha g^2\omega^{-5}\exp\left[-\frac{5}{4}\left(\frac{\omega}{\omega_p}\right)^{-4}\right]\gamma^{\delta}r(\omega_*), \tag{41}$$

in which:

$$\alpha=0.076\left(\frac{gX}{U^2}\right)^{-0.22}, \tag{42}$$

$$\omega_p=7\pi\left(\frac{g}{U}\right)\left(\frac{gX}{U^2}\right)^{-0.33}, \tag{43}$$

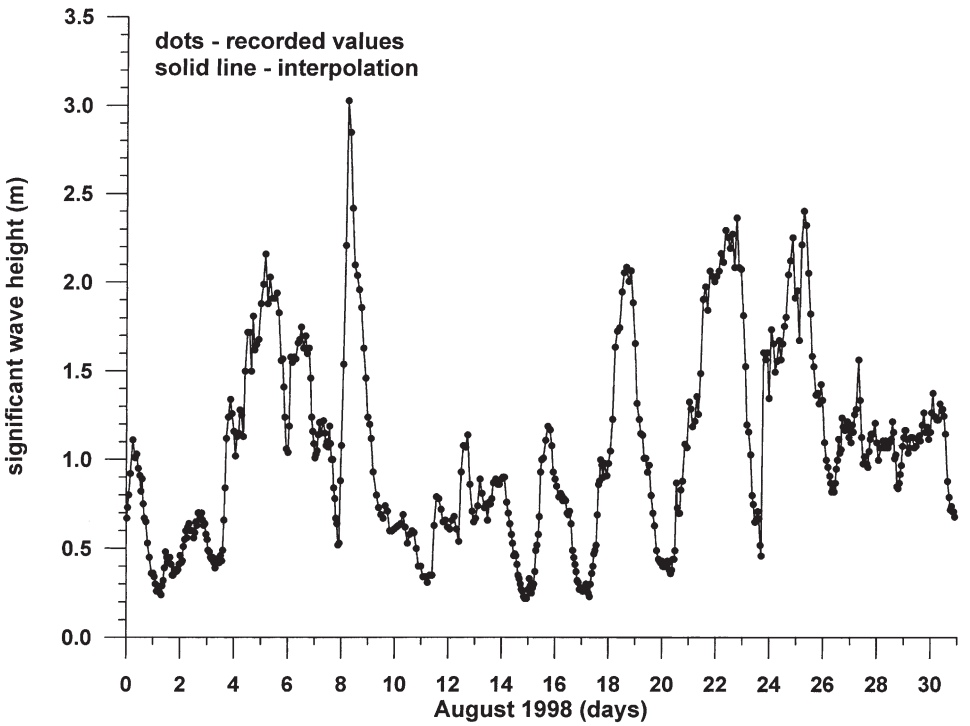

Fig. 11. Variation of significant wave height in the Baltic Sea in August 1998 (54° 51.234′N; 17° 48.352′E).

$$\delta = \exp\left[-\frac{(\omega-\omega_p)^2}{2\sigma_0^2\omega_p^2}\right]. \tag{44}$$

For the mean JONSWAP spectrum we have: γ=3.3, σ_0'=0.07 for $\omega \leq \omega_p$ and σ_0''=0.09 for $\omega > \omega_p$. The function $r(\omega_*)$ is given by (Massel, 1996):

$$r(\omega_*)=f^{-2}\left[1+\frac{2\omega_*^2 f}{\sinh(2\omega_*^2 f)}\right]^{-1}, \tag{45}$$

in which:

$$\omega_*=\omega\sqrt{\frac{h}{g}} \text{ and } f=\frac{gk}{\omega^2}. \tag{46}$$

The zeroth order moment of the JONSWAP spectrum, m_0, is related to the non-dimensional fetch as follows (Massel, 1996):

$$\frac{m_0 g^2}{U^4}=1.6\cdot 10^{-7}\left(\frac{gX}{U^2}\right), \tag{47}$$

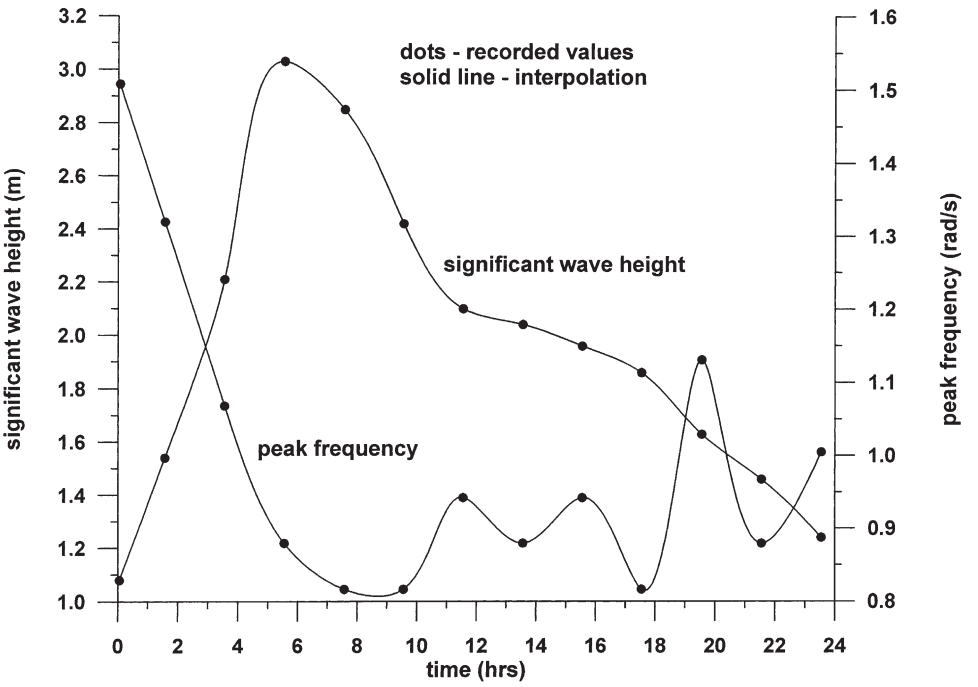

Fig. 12. Recorded and interpolated significant wave heights and peak frequencies on August 9, 1998 in the Baltic Sea (54° 51.234′N; 17° 48.352′E).

where

$$m_0=\frac{H_s^2}{16}. \tag{48}$$

Using Eqs. (42), (43), (47) and (48), it can be shown that:

$$\alpha=0.108\left(\frac{\omega_p^2 H_s}{g}\right)^{1.375}. \tag{49}$$

Full representation of the wave field requires information on the directional spreading of the wave energy. Due to the lack of measurements on the energy spreading the directional spreading is assumed in the form suggested by Donelan et al. (1985):

$$D(\Theta)=\frac{1}{2}\beta \cosh^{-2}[\beta(\Theta-\Theta_0)]. \tag{50}$$

Although the $\cosh^{-2}(\beta\Theta)$ distribution extends beyond $\pm\frac{\pi}{2}$, the spreading function

is less than 9% of its peak value at $\pm\frac{\pi}{2}$ for β larger than 1.2. In this paper, somewhat narrower spreading is used with β=3.0.

Combining Eqs. (41) and (50) we get the full directional–frequency spectrum $S_1(\omega,\Theta)$ as:

$$S_1(\omega,\Theta)=S(\omega)D(\Theta). \tag{51}$$

The simplest representation of a confused sea is the summation of many independent harmonics travelling in various directions. These harmonics are superimposed with random phase, ϕ, which is uniformly distributed on $(-\pi,\pi)$. Thus, the surface elevation is:

$$\zeta(t)=\sum_{m=1}^{M}\sum_{n=1}^{N}\alpha_{mn}\cos(\omega_m t-\phi_{mn}), \tag{52}$$

in which a_{mn} and ω_p are the amplitudes and frequencies of the spectral components, respectively. In Eq. (52), M=155 frequencies and N=180 directions were used for simulation. The frequencies are non-uniformly distributed in the frequency band $0.5\omega_p<\omega<3.0\omega_p$, while directions are distributed uniformly in the range $(-\pi,\pi)$; thus $\Delta\Theta=2°$.

In general, there are two procedures for carrying out the simulation of sea surface time series for a given spectrum. In the first procedure, the amplitudes a_{mn} of the component waves are treated as deterministic quantities derived from the simulated spectrum, i.e.:

$$a_{mn}^2=2S_1(\omega,\Theta)\Delta\omega_m\Delta\Theta_n, \tag{53}$$

where $\Delta\omega_m$ denotes the bandwidth of the mth frequency and $\Delta\Theta_n$ is the bandwidth of the nth wave angle. In the second method, the amplitudes are also treated as random variables. However, the simulations reported, for example, by Massel and Brinkman (1998) showed that both methods yield very similar results of reproducing the sea surface frequency spectra and probabilistics of density of surface ordinates, wave height and wave period. In this paper the first method is used.

6.1.3. The WT processing of reconstructed sea surface time series

The reconstructed time series is of the duration of seven hours with the typical Wave Rider Buoy sampling time Δt=0.7812 s. It gives N=32258 values of the sea surface elevation. Fig. 13 shows the resulting absolute value of the wavelet transform when scale b is in the range from 2 s to 20 s. The $|WT|$ value increases with time and its maximum value is reached at about 6 o'clock in the morning of August 9, 1998. It should be noted that the range of the scales (periods) increases when the wave field becomes more developed and the spectrum becomes wider. At the end of the calculation time, the $|WT|$ values slightly decrease. An evolution, in time, of the period and frequency, corresponding to the maximum values of the $|WT|$, is shown in Fig. 14. Although there are some high frequency oscillations of the periods

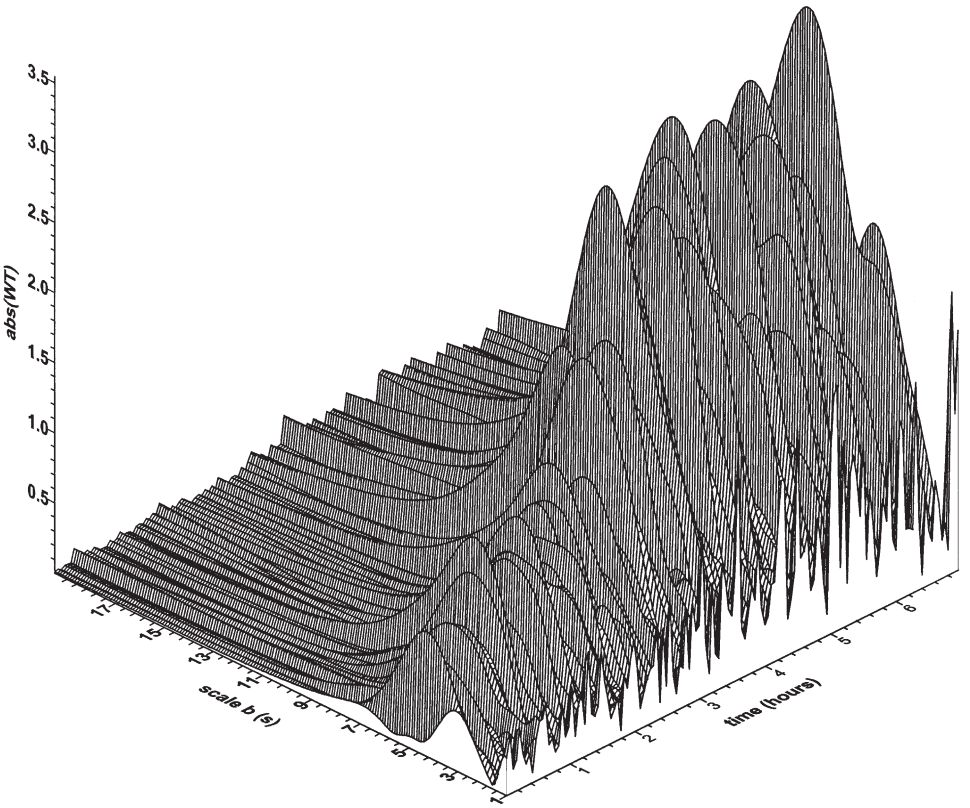

Fig. 13. The $|WT|$ surface for the reconstructed time series on August 9, 1998 in the Baltic Sea (54° 51.234′N; 17° 48.352′E).

(frequencies), the increasing (decreasing) trend is clearly seen in the figure. The maximum period (or minimum frequency) appears at about 6 o'clock in the morning of August 9, 1998 when the development of the wave field reaches its maximum (see Fig. 12).

6.2. Shallow water waves close to breaking

One minute record of wave induced velocity in very shallow water is shown in Fig. 15a. The velocity was recorded on December 5, 1997 on the top of the Ningaloo Reef (Australian coast of the Indian Ocean at S 21°48′, E 114°5′) during studies on the circulation and flushing of the reefs in this region. The velocity was measured by the InterOcean's S4 current meter located in the water depth of about 1.0 m. Superposition of the wind induced waves and oceanic swell, transforming on the steep reef slope, frequently results in the wave breaking and fast variation of the flow velocity. In particular, at time instants of about 1007 s and 1037 s, a rapid rising of velocity from about 20 cm/s to more than 1 m/s, is observed.

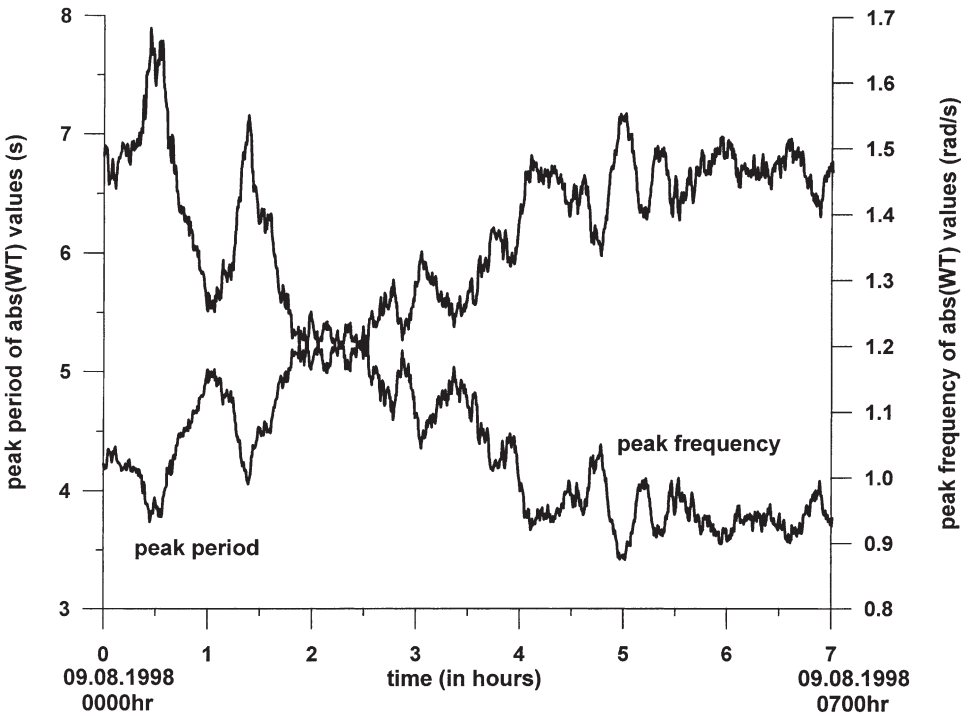

Fig. 14. Variation of the peak period and peak frequency on August 9, 1998 in the Baltic Sea (54° 51.234′N; 17° 48.352′E).

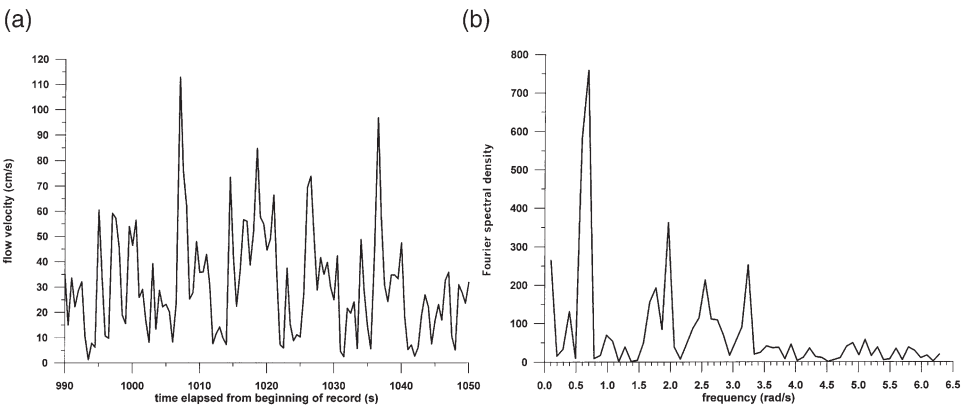

Fig. 15. One minute record of the wave induced velocities on the top of the Ningaloo Reef (Western Australia) on December 5, 1997: (a) velocity time series (b) Fourier transform.

Fig. 15b illustrates the spectral density function obtained using the classical Fourier transform. A few peaks, corresponding to the frequencies 0.16 rad/s, 0.6 rad/s, 2 rad/s, 2.55 rad/s and 3.25 rad/s, are clearly distinguished. A more complete picture, obtained by the wavelet transform, is given in Fig. 16. A sequence of the local maxima, with the periods of about 8 to 10 s, are densely distributed along whole record. These maxima correspond to the highest peak in the spectrum (see Fig. 15b). Moreover, a sequence of the smaller maxima with the periods of 2–3 s is shown. It is interesting to note that the wavelet transform is able to disclose the energy peak, with the period of about 32 s which is not so clearly seen in the classical spectrum. Comparing Figs. 15a and 16, we find that the two biggest maxima of the velocity $\approx$110 cm/s and $\approx$95 cm/s in Fig. 15a are induced by the wave components of periods $\approx$32 s and $\approx$25 s, respectively.

6.3. Disintegration of mechanically generated wave train

Two records of mechanically generated waves are presented in Fig. 17a and b. These records were obtained in the wave flume of the Institute of Hydroengineering in Gdansk, Poland (Sobierajski, 1999). The two stations, 1 and 6, were located at 4 m and 49 m from the wavemaker, respectively. The incident waves of the height

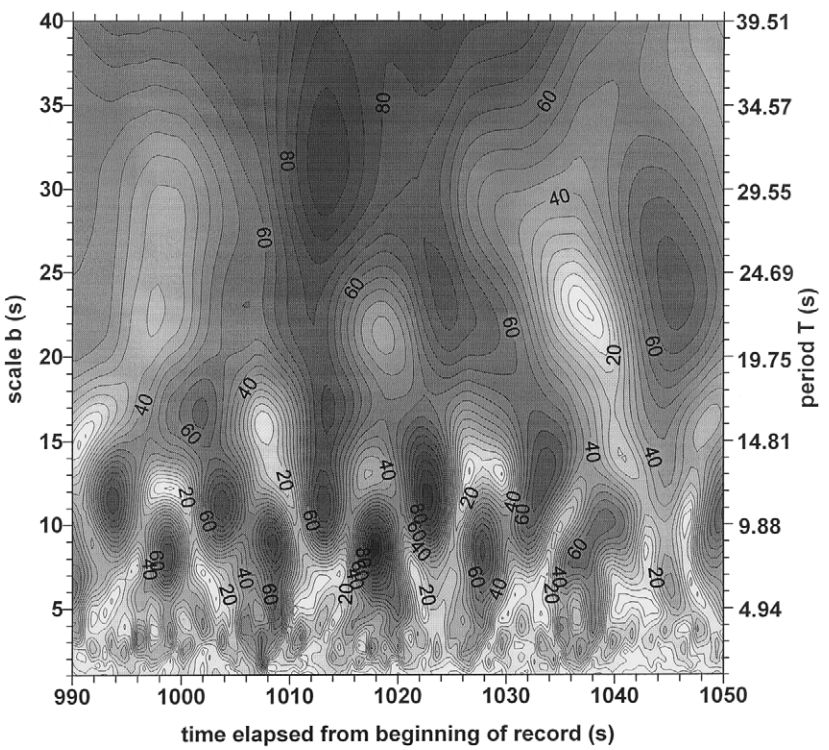

Fig. 16. Contours of the $|WT|$ for time series given in Fig. 15a.

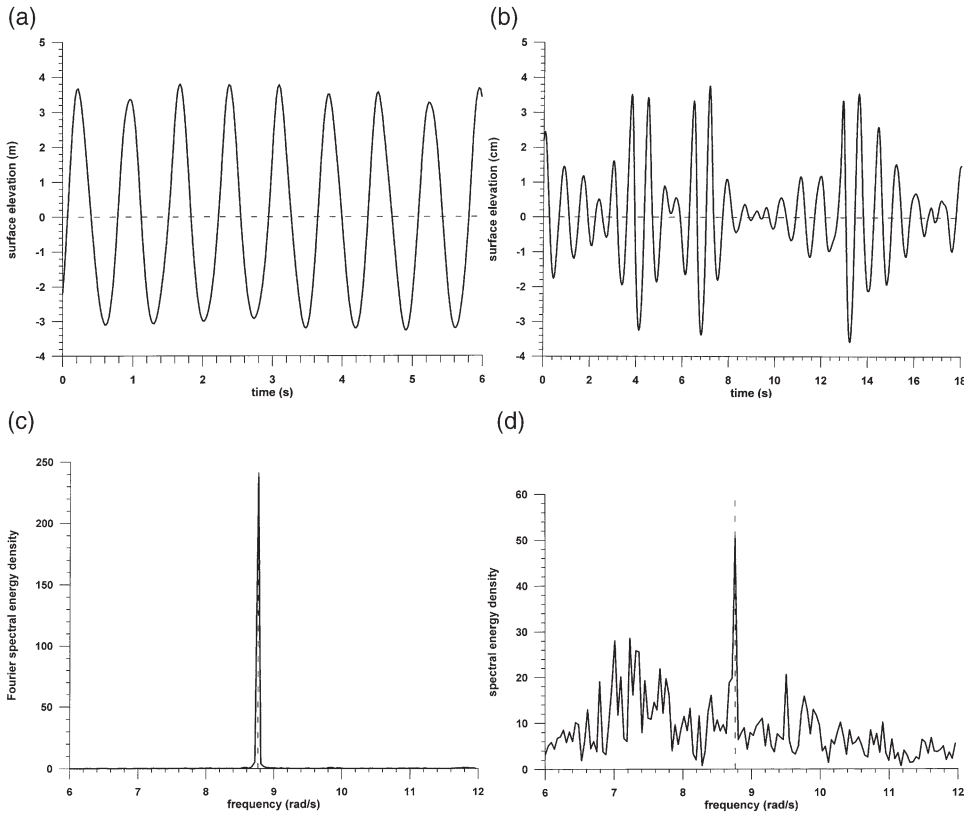

Fig. 17. Mechanically generated waves in the wave flume: (a) time series at gauge 1, (b) time series at gauge 6, (c) Fourier transform of time series given in (a), (d) Fourier transform of time series given in (b).

H=0.06 m and period T=0.717 s (frequency ω=8.76318 rad/s) were generated in water depth of 0.4 m. The comparison of both records indicates that initially sinusoidal wave train undergoes a substantial modifications with a strong grouping (see gauge 6). This signal disintegration is also clearly seen in the spectral structure of both records (Fig. 17c and d). The energy, initially concentrated at the wavemaker frequency ω=8.76318 rad/s, after propagating at a distance of 45 m, redistributes over a broad spectrum. The corresponding wavelet transform absolute value $|WT(\tau,b)|$ of the record at gauge 6 is shown in Fig. 18. The contours of $|WT(\tau,b)|$ illustrate a strong non-uniformity of the wave surface with very low energy observed for the time interval of 8 to 10 seconds.

In Fig. 19, the *global wavelet energy spectrum*, E_3, for gauge 6 is shown. The maximum of the spectrum is slightly shifted from the wavemaker frequency towards the low frequencies probably due to the fact that more energy was "pumped" into the lower frequencies than towards the higher frequencies.

In any steady periodic wave train, which is nonlinear in general, there must also be present harmonics of the fundamental frequency. If we introduce a small disturb-

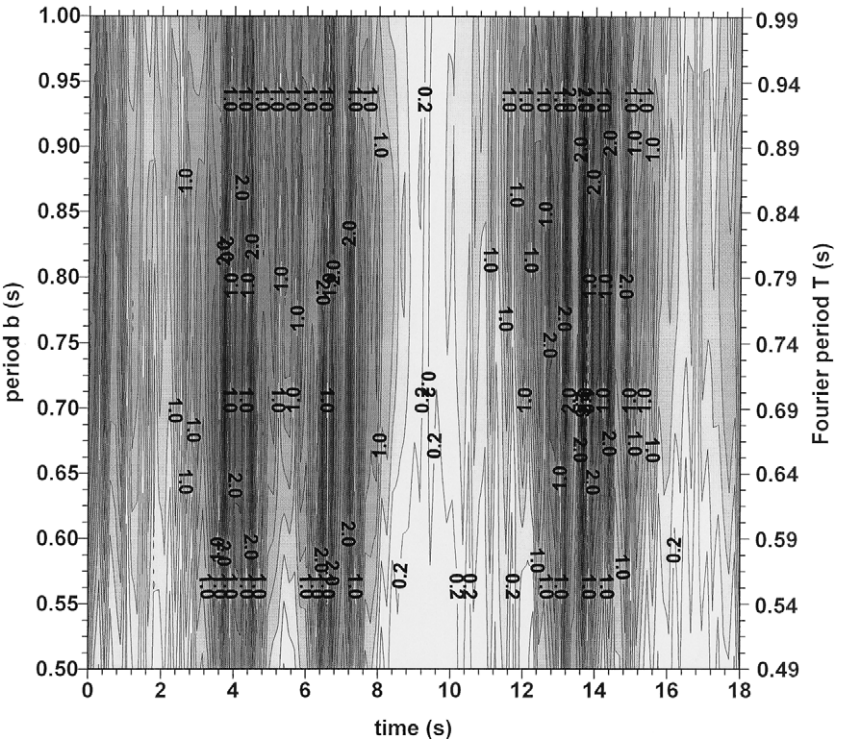

Fig. 18. Wavelet transform contour for time series given in Fig. 17b.

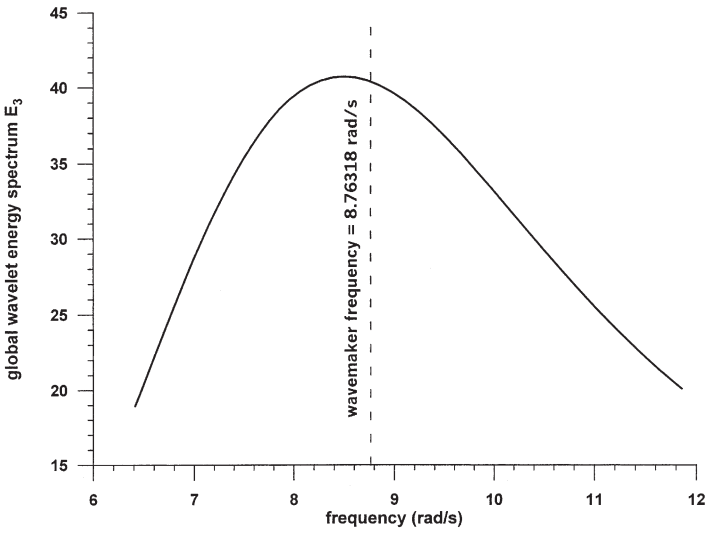

Fig. 19. Global wavelet energy spectrum E_3 for time series given in Fig. 17b.

ance in the form of two modes with "side-band" frequencies, adjacent to the fundamental frequency, due to nonlinear interaction mechanism, the side-band modes will be forced to increase exponentially. The primary wave motion becomes unstable to this form of disturbance. This kind of instability of periodic wave trains is known as the Benjamin–Feir instability (Benjamin and Feir, 1967; Benjamin, 1967). In particular, Benjamin (1967) showed that the instability appears when:

$$kh > 1.363, \text{ or } L < \frac{2\pi}{1.363} h = 4.61h, \tag{54}$$

where k is the wave number, h is the water depth and L is the wavelength. In our case, L=0.8 m and h=0.4 m. Thus, L=0.8<4.61 h=1.844 m, and the wave train in the flume, after travelling many wavelengths, becomes unstable.

7. Conclusions

This paper deals with some fundamentals of the wavelet transform, being a new technique of processing of the experimental time series. This technique is particularly suitable for non-stationary processes. In contrast to the Fourier transform, the wavelet transform allows exceptional localization, both in the time domain via translation τ of the wavelet, and in the frequency domain via dilations scales b, which can be changed from minimum to maximum, chosen by the user. The wavelet transform is not intended to replace the Fourier transform which remains very appropriate in the study of the stationary signals when there is no need for local information.

The simple examples demonstrate the WT's capability to give a full time–frequency representation of the wave signal. The processing of the time series resulting from recording the wind induced deep water waves, waves breaking on the tropical coral reefs and mechanically generated waves in the wave flume demonstrates the ability of the WT technique to detect the complex variability of these signals in time–frequency space.

In particular for deep water waves, the wavelet transform reveals the wave energy growth and widening of the frequency domain during the six hours of the generation stage. The variations of the frequencies corresponding to the maximum of the wavelet transform at particular time are very similar to the recorded frequencies. In this paper, in the case of the rapidly changing wave-induced velocity due to wave transformation on the steep coral reef, we demonstrate the application of the WT technique for a strongly non-stationary hydrodynamic process. It is interesting to note that wavelet transform shows the influence of the some low frequency components which are not clearly seen in the classical energy spectrum. Finally, the WT method helps to examine a process of the disintegration of mechanically generated waves. As was shown, this disintegration corresponds to the Benjamin–Feir instability mechanism.

Acknowledgements

The author wishes to thank Dr. B. Paplinska and Dr. E. Sobierajski from the Institute of Hydroengineering, Gdansk, Poland for the deep water and wave flume wave data. Mr. R. Brinkman from the Australian Institute of Marine Science is gratefully acknowledged for providing the velocity data from the Ningaloo Reef, Australia.

References

Bendat, J.S., Piersol, A.G., 1986. Random data. Analysis and Measurement Procedures. John Wiley and Sons, New York.

Benjamin, T.B., 1967. Instability of periodic wave trains in nonlinear dispersive systems. Proceedings of the Royal Society A 299, 59–75.

Benjamin, T.B., Feir, J.E., 1967. The disintegration of wave train on deep water. Part 1: Theory. Journal of Fluid Mechanics 27, 417–442.

Combes, J.M., Grossman, A., Ychamitchian, P. (Eds.), 1989. Wavelets. The Time-Frequency Methods and Phase Space. Springer-Verlag, Berlin, Heidelberg.

Daubechies, I., 1992. Ten Lectures on wavelets. Society for Industrial and Applied Mathematics.

Donelan, M.A., Hamilton, J., Hui, W.H., 1985. Directional spectra of wind-generated waves. Philosophical Transaction Royal Society 315, 509–562.

Emery, W.J., Thomson, R.E., 1997. Data Analysis Methods in Physical Oceanography. Pergamon Press, Oxford.

Farge, M., 1992. Wavelet transform and their applications to turbulence. Annual Review of Fluid Mechanics 24, 395–457.

Gamage, N., Blumen, W., 1993. Comparative analysis of low-level cold fronts: wavelet, Fourier, and empirical orthonormal function decomposition. Monthly Weather Review 21, 2867–2878.

Kaiser, G., 1994. A Friendly Guide to Wavelets. Birkhauser, Boston.

Liu, P.C., 1995. Wavelet spectrum analysis and ocean wind waves. In: Foufoula, G., Kumar, P. (Eds.), Wavelets in Geophysics. Academic Press, pp. 151–166.

Massel, S.R., 1996. Ocean Surface Waves: Their Physics and Prediction. World Scientific Publications, Singapore, New York.

Massel, S.R., 1999. Fluid Mechanics for Marine Ecologists. Springer Verlag, Berlin, Heidelberg.

Massel, S.R., Brinkman, R.M., 1998. On the determination of directional wave spectra for practical applications. Applied Ocean Research 20, 357–374.

Meyer, Y., Jaffard, S., Rioul, O., 1987. L'analyse par ondelettes. Pou la Science, Sept., pp. 28–37.

Meyers, S.D., Kelly, B.G., O'Brien, J.J., 1993. An introduction to wavelet analysis in oceanography and meteorology with application to the dispersion of Yanai waves. Monthly Weather Review 121, 2858–2866.

Mori, N., Yasuda, T., 1994. Orthonormal wavelet analysis for deep-water breaking waves. Proc. 24th Conf. On Coastal Eng., ASCE, Kobe, Japan 1, 412–426.

Paplinska, B., 1999. Wave analysis at Lubiatowo and in the Pomeranian Bay based on measurements from 1997–1998 — comparison with modelled data (WAM4 model). Oceanologia 41, 241–254.

Percival, D.P., 1995. On estimation of the wavelet variance. Biometrika 82, 619–631.

Shen, Z., Mei, L., 1993. Equilibrium spectra of water waves forced by intermittent wind turbulence. Journal of Physical Oceanography 23, 2019–2026.

Shen, Z., Mei, L., 1994. Fine structure of wind wave analyzed with wavelet-transform. Journal of Physical Oceanography 24, 1085–1094.

Sobierajski, E., 1999. Initial wave studies in the new wave flume. Intern. Report, Institute of Hydroengineering, Gdańsk, (in Polish).

Torrence, C., Compo, G.P., 1998. A practical guide to wavelet analysis. Bulletin of the American Meteorological Society 79, 61–78.

Tuteur, F.B., 1989. Wavelet transformations in signal detection. In: Combes, J.M., Grossman, A., Ychamitchian, P. (Eds.), Wavelets. The Time-Frequency Methods and Phase Space. Springer-Verlag, Berlin, Heidelberg, pp. 132–138.

Van Name, F.W., 1960. Modern Physics. Prentice-Hall, Inc, Englewood Cliffs.

Yamada, M., Ohkitani, K., 1990. Orthonormal wavelet expansion and its application to turbulence. Prog. Theor. Phys. 83, 819–823.

Yamada, M., Ohkitani, K., 1991. An identification of energy cascade in turbulence by orthonormal wavelet analysis. Prog. Theor. Phys. 86, 799–815.